JOURNAL OF AIRCRAFT
Vol. 39, No. 3, May–June 2002

Comparing Fatigue Life Estimates Using Experimental and Spectral Density Based Probability Distributions

S. M. Spottswood* and H. F. Wolfe†
U.S. Air Force Research Laboratory, Wright–Patterson AFB, Ohio 45433-7006

Random vibration, high-cycle fatigue problems in thin-skinned structures are of concern to the U.S. Air Force. Therefore, the U.S. Air Force is interested in available methods used to approximate the response and fatigue life of aircraft structures exposed to random vibration loading, notably those exhibiting geometric nonlinear effects. The purpose of this investigation is to examine and compare the fatigue life estimates of a fully clamped aluminum plate under the influence of random electrodynamic shaker loading. The experimental strain probability density function was generated using the rain flow cycle counting technique, and the resulting fatigue estimates were compared with spectral-based finite element analysis (FEA) and experimental random response fatigue estimates (Anzai, Hiroyuki, "Algorithm of the rainflow method," *The International Symposium on Fatigue Damage Measurement and Evaluation under Complex Loading*, OND Sokkic, Ltd., July 1991; Bannantine, J. A., Comer, J. J., and Handrock, J. L., *Fundamentals of Metal Fatigue Analysis*, Prentice–Hall, Inc., Upper Saddle River, NJ, 1990, pp. 193–196). The plate was modeled using the ABAQUS® linear random response algorithm and a modified nonlinear FEA code developed by Mei et al. of Old Dominion University (Dhainaut, J. M., Bin, D., Mei, C., Spottswood, S. M., and Wolfe, H. F., "Non-Linear Response of Composite Panels to Random Excitation and Elevated Temperature," *Structural Dynamics: Recent Advances*, Univ. of Southampton, U.K., 2000; Shi, Y., and Mei, C., "A Finite Element Time Domain Modal Formulation for Large Amplitude Free Vibrations of Beams and Plates," *Journal of Sound and Vibration*, Vol. 193, No. 2, 1996, pp. 453–464). For all scenarios the Palmgren–Miner linear damage accumulation model was utilized (Miner, M. A., "Cumulative Damage in Fatigue," *Journal of Applied Mechanics*, Vol. 67, 1945, pp. A159–A182). This simple isotropic plate case was selected as a means for accurate assessment, as opposed to using a more complex structure initially. Results indicate that the spectral-density-based analyses provide overly conservative fatigue life estimates when compared with the experimental based fatigue life estimates.

Introduction

THE probability density function (PDF) determined from the experimental time record, along with Miner's cumulative damage theory[1] and the material constants from a random stress vs cycles to failure, or S-N curve, provided the ability to estimate the fatigue life of the aluminum plate. Using the finite element analysis (FEA) random response results, the Dirlik spectral-based technique was used to estimate the PDF from the moments of the respective random response stress power spectral densities (PSD).[2] The Miner cumulative damage model was used, with the spectral based PDF, to estimate the fatigue life. Finally, because the Dirlik technique is independent of PSD input the strain response PDF was also approximated using the PSD generated from the experimental time record, as the basis for comparing the FEA-derived PDF estimates. The experimental geometric nonlinear response of thin-skinned structures is well documented in the literature.[3–7] It is also known that the nonlinearities in question, that is, peak-broadening and frequency shifting, can be captured analytically by considering the nonlinear stiffness.[8–11] Thus, the use of both the linear ABAQUS® and nonlinear codes allowed for a comparison of response and fatigue life predictions, noting the effect of considering geometric nonlinear stiffness in the analysis.

Presented as Paper 2001-1609 at the AIAA/ASME/ASCE/AHS/ASC 42nd Structures, Structural Dynamics, and Materials Conference and Exhibit, Seattle, WA, 16–19 April 2001; received 11 June 2001; revision received 10 October 2001; accepted for publication 12 December 2001.

*Aerospace Engineer, AFRL/VASS Building 24C, 2145 5th Street, Suite Z. Member AIAA.
†Senior Aerospace Engineer. Member AIAA.

Background

Experimental Procedure

Experimental random vibration tests were conducted on clamped, 8.0-in. (203-mm) by 10.0-in. (254-mm) by 0.061-in. (1.55-mm), 7075-T6 aluminum plates, using a 20,000-lb_f electrodynamic shaker. By electrodynamically exciting the clamping fixture, an inertial load was imparted to the plate. The clamp was manufactured with a radius of curvature of 4.75 mm around the plate/clamp interface to reduce early fatigue. The response of the plates was monitored using Measurements Group, Inc., WK-00-125AD-350 strain gauges, labeled 1–8 displayed in Fig. 1, and a Vibra-Metrics, Inc., 1000A piezoelectric accelerometer mounted on the shaker armature. The strain gauges have a transverse sensitivity of $-2.10 \pm 0.2\%$. Because the transverse strain was not experimentally measured along the clamp/panel interface, an estimate of the experimental error was obtained utilizing the ratio of transverse to axial strain from a nonlinear ABAQUS static analysis. Consistent discretization and elements were used for both the static and dynamic study. For the static case a transverse displacement, equal to the plate thickness, was prescribed in the plate center. In the location of gauge 7, the resulting transverse sensitivity error was quite small, estimated to be -0.66%.

A sampling rate of 8000 samples per second was used throughout the test effort. Two panels were fatigue tested at a target strain level of 560 $\mu\varepsilon$ rms, measured at strain gauges 3 and 7. The corresponding input acceleration level, required for that strain level, was 4.0 g^2/Hz over the frequency bandwidth, 100–1000 Hz, or 60-g rms. Cumulative rms strain gauge measurements for gauge 7 are shown in Fig. 2. A 10-s time step was used to compute the rms strain values of successively larger time records from the strain time history. As the time record length increased, the rms strain value converged. Figure 2 was used to determine what data record length was required for the formulation of the experimental PSD and rain-flow PDF. Previous studies demonstrated the wide variability of the rms strain and resulting fatigue life estimates, prior to the convergence

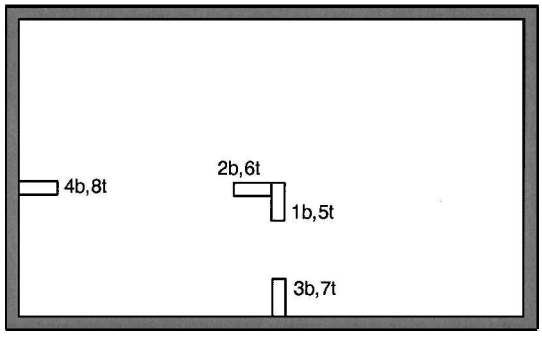

Fig. 1 Clamped 8 × 10 in. 7075 T6 aluminum plate, displaying strain gauge location (t = top; b = bottom).

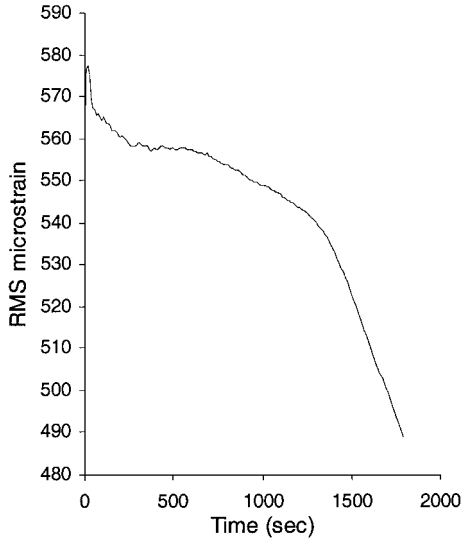

Fig. 2 Strain gauge 7 cumulative rms strain time history.

of the data record.[12] In a random vibration problem such as this, stationarity is assumed in order to characterize the PSD and PDF as representative of the entire load history. For this analysis a rms convergence criterion of 0.1% was used, resulting in the use of the first 100 s of the time record. Figure 3 was used to determine the time to failure for the aluminum panel. The panel fundamental frequency was recorded every 60 s, and a higher-order polynomial curve was fit to the data. For this study a 5% reduction in fundamental frequency was used to determine the fatigue life of the panel. Using the aforementioned criterion, time to failure was estimated as 1270 s for both panels. Figure 4 displays panel 2 at the end of the 30-min test, having undergone a dye-penetrant nondestructive evaluation. Damage in the form of cracks is evident along each of the clamped plate boundaries.

Linear Finite Element Modeling

Modeling conducted using ABAQUS incorporated S8R5, eight-node rectangular plate elements with an edge length of 0.1 in. (2.54 mm). The 7075-T6-aluminum panel material properties, used in the FEA modeling, were a density of 0.101 $lb_m/in.^3$ (2796 kg/m^3) and an elastic modulus of 10.4E6 $lb_f/in.^2$ (71.71 GPa). Boundary conditions for the plate are shown in Fig. 5a. Rotational stiffness, modeled using 0-D grounded/torsional spring elements at the respective clamped boundaries, was added in order to more closely approximate the experimental natural frequencies of the plate. In addition, structural damping was defined for the dominant modes (1,1), (3,1), and (1,3), as 0.58, 0.05, and 0.25%, respectively. The experimental random shaker input was modeled using ABAQUS random response base motion with flat input PSDs. The linear random response algorithm uses the results from a normal modes analysis step. Input levels included 0.0025 g^2/Hz and the fatigue test level of 4.0 g^2/Hz, over the frequency bandwidth 100–1000 Hz.

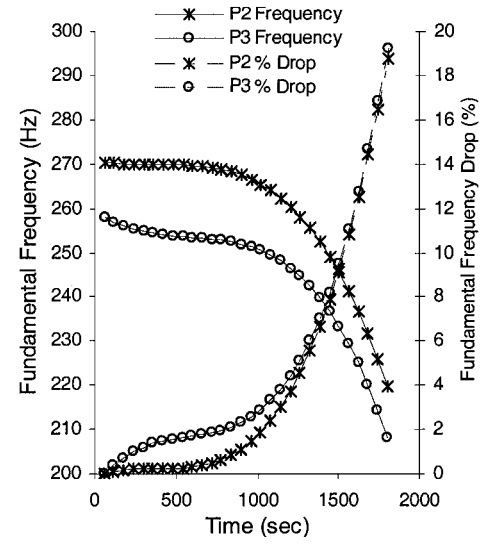

Fig. 3 Fundamental frequency and corresponding frequency shift of strain gauge 1 caused by the onset of damage in panel 2 (P2) and panel 3 (P3).

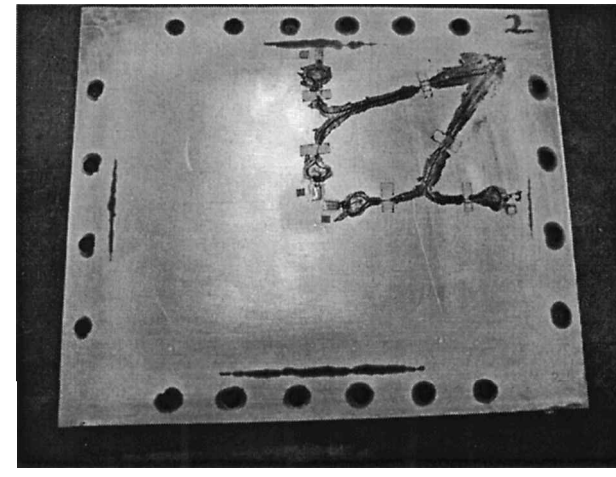

Fig. 4 Damaged panel 2 at the end of the 30-min test, illustrating edge cracks at each of the clamped boundaries.

The strain time history used in the experimental data analysis was recorded using strain gauge 7, located at the midpoint of the 10.0 in. edge, perpendicular to the clamp, as shown in Fig. 5a. Similarly, the FEA strain response was measured in the x direction, relative to the coordinate system also depicted in Fig. 5a.

Nonlinear Finite Element Formulation/Modeling

Modeling using the nonlinear FEA code was conducted using four-node, 24-degree-of-freedom (DOF) C^1 rectangular plate elements, where C^1 implies interelement continuity for the DOF and its first derivatives.[13] Instead of clamped boundary conditions, rotational stiffness was added to the linear stiffness matrix to better approximate the experimental test conditions. The same material properties as those used in the linear model were also used in this model. A brief summary of the geometric nonlinear development follows, with a complete derivation outlined by Mei et al.[8,9] The governing nonlinear equations of motion were originally developed for a laminated composite plate subjected to both thermal and acoustic loads. For the purposes of this comparison, inertial loading was used in the place of acoustic loading. Furthermore, all testing was conducted at ambient conditions; therefore, the thermal loading derived by Mei et al. was neglected.[8,9] What follows is a brief overview of the strain-displacement and constitutive relations. Von Kármán

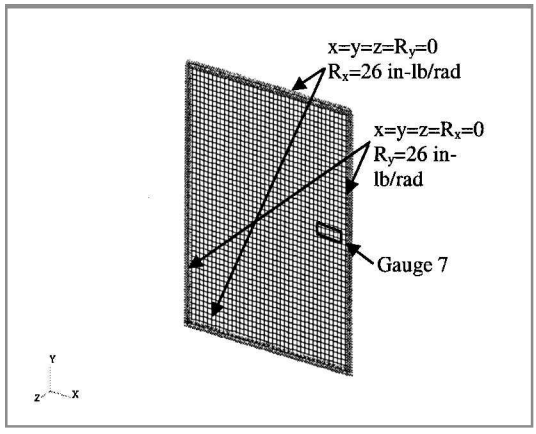

a)

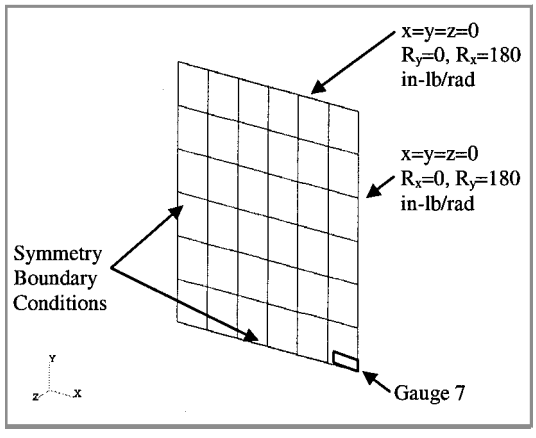

b)

Fig. 5 Boundary conditions for a) ABAQUS and b) nonlinear, $\frac{1}{4}$-plate model.

strain-displacement relations are expressed as follows:

$$\{\varepsilon\} = \begin{Bmatrix} \varepsilon_x \\ \varepsilon_y \\ \gamma_{xy} \end{Bmatrix} = \begin{Bmatrix} u_{,x} \\ v_{,y} \\ u_{,y} + v_{,x} \end{Bmatrix} + \begin{Bmatrix} w_{,x}^2/2 \\ w_{,y}^2/2 \\ w_{,x} w_{,y} \end{Bmatrix} + z \begin{Bmatrix} -w_{,xx} \\ -w_{,yy} \\ -2w_{,xy} \end{Bmatrix}$$

$$= \{\varepsilon_m^0\} + \{\varepsilon_b^0\} + z\{\kappa\} \tag{1}$$

where $\{\varepsilon_m^0\}$ and $\{\varepsilon_b^0\}$ are the strain components corresponding to the in-plane and transverse deflection. The laminate constitutive equations, relating the resultant forces and moments to the strain expressions, are expressed as

$$\begin{Bmatrix} N \\ M \end{Bmatrix} = \begin{bmatrix} A & B \\ B & D \end{bmatrix} \begin{Bmatrix} \varepsilon^0 \\ \kappa \end{Bmatrix} \tag{2}$$

where $[A]$, $[B]$, and $[D]$ are the elastic in-plane, extension-bending, and flexural rigidity stiffness matrices, respectively. Using Hamilton's principle and the finite element formulation, the element nonlinear equations of motion, indicated in lowercase letters, were expressed as

$$\begin{bmatrix} [m_b] & 0 \\ 0 & [m_m] \end{bmatrix} \begin{Bmatrix} \{\ddot{w}_b\} \\ \{\ddot{w}_m\} \end{Bmatrix} + \left(\begin{bmatrix} [k_b] & [k_B] \\ [k_B^T] & [k_m] \end{bmatrix} \right) \begin{Bmatrix} \{w_b\} \\ \{w_m\} \end{Bmatrix}$$

$$+ \left(\begin{bmatrix} [k_{1\,\mathrm{Nm}} + k_{1\,\mathrm{NB}}] & [k_{1\,\mathrm{bm}}] \\ [k_{1\,\mathrm{mb}}] & 0 \end{bmatrix} + \begin{bmatrix} [k_{2b}] & 0 \\ 0 & 0 \end{bmatrix} \right)$$

$$\times \begin{Bmatrix} \{w_b\} \\ \{w_m\} \end{Bmatrix} = \begin{Bmatrix} \{p(t)\} \\ 0 \end{Bmatrix} \tag{3}$$

where $[m]$ and $[k]$ are the element mass and linear stiffness matrices, $\{w_m\}$ is the in-plane nodal vector, and $\{w_b\}$ the transverse displacement nodal vector.[8,9] Matrices $[k_1]$ and $[k_2]$ correspond to first- and second-order nonlinear stiffness terms. The subscripts B, Nm, and NB refer to the stiffness contributions that correspond to the laminate extension bending $[B]$ and in-plane force components defined in Eq. (2). Because an isotropic specimen was studied, the laminate coupling stiffness matrices $[k_B] = [k_{1\,\mathrm{NB}}] = 0$ and extension-bending matrix $[B] = 0$. As already discussed, the load vector $\{p(t)\}$ represents the time varying inertial loading. Assembling the elements for the plate model and applying the kinematic boundary conditions, the system equations of motion in structural node DOF were expressed as

$$[M]\{\ddot{W}\} + ([K] + [K_1] + [K_2])\{W\} = \{P(t)\} \tag{4}$$

where $[M]$, $[K]$, and $\{P(t)\}$ denote the system mass, linear stiffness matrices, and inertial load or base acceleration vector, respectively, whereas $[K_1]$ and $[K_2]$ denote the first- and second-order nonlinear stiffness matrices, which depend linearly and quadratically on the relative displacement $\{W\}$.[8,9] Because the specimen of concern was excited using base motion, the inertial load vector $\{P(t)\}$ was defined as

$$\{P(t)\} = -[M]\{\ddot{z}\} \tag{5}$$

where $\{\ddot{z}\}$ is the base acceleration vector and $[M]$ is the system mass matrix.

After neglecting the membrane inertia term $\{\ddot{w}_m\}$, solving for $\{w_m\}$, and substituting the resulting expression back into Eq. (3), the system equations of motion, indicated in capital letters, were expressed in terms of the relative transverse displacement vector $\{w_b\}$ as

$$[M_b]\{\ddot{W}_b\} + ([K_b])\{W_b\} + [K_{1\,\mathrm{Nm}}]\{W_b\}$$

$$+ \left([K_{2b}] - [K_{1\,\mathrm{bm}}][K_m]^{-1}[K_{1\,\mathrm{mb}}] \right)\{W_b\} = \{P(t)\} \tag{6}$$

Mei et al. transformed the system equations of motion from physical into modal coordinates. This step increases computational efficiency by significantly reducing the number of DOF.[8,9] This was accomplished using the following modal transformation:

$$\{W_b\} = \sum_{r=1}^{n} q_r(t)\{\phi_b\}^{(r)} = [\Phi]\{q\} \tag{7}$$

where r is the number of retained linear modes and $\{\phi_b\}^{(r)}$ is the normal mode of the system linear vibration solution. Finally, after completing the modal transformation and introducing modal damping ξ_r the system equations of motion reduce to a set of nonlinear, coupled modal equations:

$$[\bar{M}]\{\ddot{q}\} + 2\xi_r \omega_r \bar{M}_r[I]\{\dot{q}\} + ([\bar{K}_L] + [\bar{K}_{qq}])\{q\} = \{\bar{P}\} \tag{8}$$

where $[\bar{M}]$ is the modal mass matrix, $[\bar{K}_L]$ is the linear stiffness matrix, $[\bar{K}_{qq}]$ is cubic in $\{q\}$, and $\{\bar{P}\}$ is the modal random inertial load vector. The solution, in the form of the relative transverse displacement, was determined using experimental acceleration time-history input and a Runge–Kutta numerical integration scheme. The time step used in the nonlinear analysis numerical integration, 1.25E-4 s, was limited by the experimental sampling rate.

Fatigue Life Estimates

The Miner linear damage accumulation model was selected to characterize the fatigue life of the 7075-T6 aluminum plate specimens and is expressed in the following equation:

$$N_t = \left[\sum \frac{P(S)}{N} \right]^{-1} \tag{9}$$

where N_t is the total number of cycles to failure, $P(S)$ is the peak stress probability density function, and N is the total number of

cycles to failure at incremental constant amplitude strain levels.[14] Expressing Eq. (9) in terms of hours results in the following:

$$t(\mathrm{s}) = \left\{ \left[\sum \frac{P(S)}{N} \right] f_c \right\}^{-1} \tag{10}$$

where N is the total number of cycles to failure at a specified stress level and f_c is the cyclic frequency. For a single mode case the cyclic frequency is taken to be the natural frequency being excited. For a multimodal case, as in this analysis, the multimodal cyclic frequency f_{cm} was taken to be the ratio of the number of peaks in the respective time-history record, to the sample time.[14] ε-N or S-N reverse bending curves on a log-log plot are characterized linearly using the following expression:

$$S = [K/N]^{\alpha} \tag{11}$$

where K and α are material property constants. Finally, substituting Eq. (11) into (10) and using the multimodal cyclic frequency yields the following relation:

$$t(\mathrm{s}) = \left\{ \left[\sum \frac{P(S)}{K/(S)^{1/\alpha}} \right] f_{\mathrm{cm}} \right\}^{-1} \tag{12}$$

where the fatigue life in seconds is defined in terms of the stress S and the material properties K and α.

The Dirlik technique is an attempt to estimate a PDF directly from the stress spectral density output.[2] It is an empirical tool used to estimate the fatigue life without the need for peak or cycle counting and therefore can be used in conjunction with finite element analysis to estimate directly fatigue life. This technique uses the moments of a PSD, where the ith moment of the PSD is defined as follows:

$$m_i = \int_0^{\infty} f^i \cdot G(f)\, \mathrm{d}f \tag{13}$$

m_i is the ith moment, f is frequency, and $G(f)$ is the power spectral density function. The rms of the response is defined as

$$\mathrm{rms} = \sqrt{m_0} \tag{14}$$

where m_0 is the zeroth moment. The peak rate, or peaks per unit time, is defined as

$$E(P) = \sqrt{m_4/m_2} \tag{15}$$

where m_2 and m_4 are the second and fourth moments, respectively. The Dirlik probability density function for rain-flow ranges is defined, in terms of the normalized stress parameter Z, as follows:

$$P(S) = \frac{(D_1/Q)e^{(-Z/Q)} + (D_2/R^2)e^{(-Z^2/2R^2)} + D_3 Z e^{(-Z^2/2)}}{2\sqrt{m_0}} \tag{16}$$

where

$$\gamma = \frac{m_2}{\sqrt{m_0 m_4}}, \qquad x_m = \frac{m_1}{m_0}\sqrt{\frac{m_2}{m_4}}$$

$$D_1 = \frac{2(x_m - \gamma^2)}{1+\gamma^2}, \qquad D_2 = \frac{\left(1 - \gamma - D_1 + D_1^2\right)}{1-R}$$

$$D_3 = 1 - D_1 - D_2, \qquad Q = \frac{1.25(\gamma - D_3 - (D_2 R)}{D_1}$$

$$R = \frac{\gamma - x_m - D_1^2}{1 - \gamma - D_1 + D_1^2}, \qquad S = 2\sqrt{m_0} Z \tag{17}$$

S is the stress range, and γ, the irregularity factor, is the ratio of the expected number of zero crossings to the expected number of peaks. The irregularity factor varies between 0 and 1, where 1 signifies a narrowband response and 0 a wide-band response. Given the probability density function of stress ranges $P(S)$, the fatigue life is estimated using Eq. (12) with the following substitutions:

$$t(\mathrm{s}) = \left\{ \left[\sum \frac{P(S)}{K/(S)^{1/\alpha}} \right] E(P) \right\}^{-1} \tag{18}$$

Results and Discussion

The boundary conditions for the ABAQUS and nonlinear FEA models are shown in Figs. 5a and 5b. A 6×6 mesh, $\frac{1}{4}$-plate model, utilizing symmetry and the aforementioned "relaxed" boundary conditions, was used in the nonlinear analysis. The mesh refinement was consistent with previous analyses conducted with this nonlinear technique.[8] Note the comparison between the theoretical and analytical natural frequencies for a simply supported panel with the respective discretization, exhibited in Table 1. The differences between the nonlinear and theoretical results were deemed an acceptable tradeoff between accuracy and the reduced-order, nonlinear analysis computational time. The first three symmetric mode shapes were used in the nonlinear analysis to transform the equations of motion from physical to modal coordinates. Figures 6a–6c depict the (1,1), (3,1), and (1,3) mode shapes. Both the linear and nonlinear FEA algorithm with torsional boundary conditions resulted in the (1,1), (3,1), and (1,3) mode shapes occurring at 220, 711, and 1000 Hz, respectively. The value of the torsional spring constant was determined by equating the FEA and experimental fundamental frequencies.

Strain response for the FEA and experimental analysis is shown in Figs. 7 and 8 for the baseline and fatigue excitation cases, 0.0025 and 4 g^2/Hz, respectively. As already mentioned, the first 100 s of the data record were used to generate the experimental PSDs. The accelerometer installed on the shaker armature provided the acceleration time-history input for the nonlinear FEA program of Mei et al.[8,9] Eight seconds of accelerometer time-history data were used in the nonlinear analysis with a time step of 1.24E-4 s using a Runge–Kutta numerical integration scheme. The ABAQUS linear random response was calculated using flat input acceleration PSDs at the aforementioned baseline and fatigue levels. The baseline case, Fig. 7, was used to establish the ABAQUS and nonlinear old Dominion University (ODU) FEA boundary conditions and structural damping. Once the model was tuned, the boundary conditions and damping parameters were held constant for the fatigue test case.

Examining Fig. 8, notice the peak broadening and shifting seen in the experimental and nonlinear FEA response. The broadening nonlinear phenomenon results from the increasing significance of

Table 1 Analytical natural frequencies for simply supported panel

Mode	(1,1)	(3,1)	(1,3)	(3,3)
Theoretical	152.46 Hz	628.41 Hz	896.14 Hz	1372.1 Hz
ABAQUS®	152.43 Hz	628.02 Hz	895.33 Hz	1370.2 Hz
ODU/nonlinear	152.78 Hz	629.23 Hz	896.83 Hz	1375.2 Hz

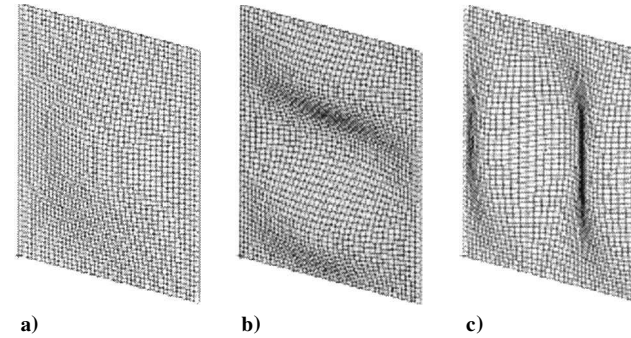

a) b) c)

Fig. 6 Mode a) (1,1); b) (3,1); c) (1,3).

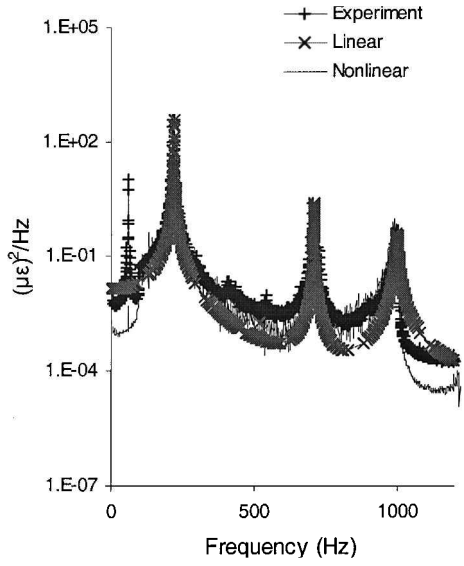

Fig. 7 Experimental (39.5 $\mu\varepsilon$ rms) vs linear (27.8 $\mu\varepsilon$ rms) vs nonlinear (37.3 $\mu\varepsilon$ rms) strain frequency response to 1.5-g rms inertial load.

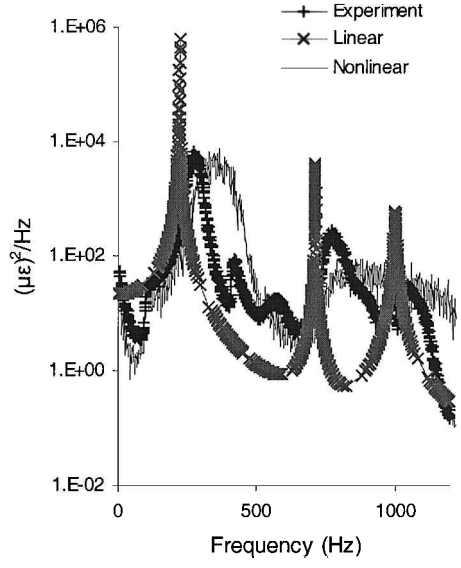

Fig. 8 Experimental (563 $\mu\varepsilon$ rms) vs linear (1113 $\mu\varepsilon$ rms) vs nonlinear (737 $\mu\varepsilon$ rms) strain frequency response to 60-g rms inertial load.

the panel membrane response.[10,11] In addition, notice that the linear FEA analysis does not characterize the response in this manner. Subsequently, the linear FEA response at the fatigue test level is significantly greater than the experimental rms strain response. However the nonlinear FEA analysis, cubic in the relative transverse displacement, does exhibit this frequency broadening and shifting. At the low-level excitation scenario the experimental, linear, and nonlinear FEA rms strain results follow: 39.5, 27.8, and 37.3 $\mu\varepsilon$, respectively. The linear FE analysis resulted in an estimate approximately 30% too low, whereas the nonlinear and experimental results compared quite favorably, with the nonlinear rms estimate only 5.5% too low. The experimental and FEA rms strain response values from the fatigue case differed significantly. The experimental, ABAQUS, and nonlinear FEA results for the fatigue loading, or the 60-*g* case, were 562.9, 1113, and 737 $\mu\varepsilon$, respectively, with the linear and nonlinear rms estimates overpredicting the response 100 and 31%, respectively.

The PDFs resulting from the experimental data and finite element analyses are displayed in Fig. 9. The PDF labeled "Experiment Rainflow" was calculated using the 100-s time record and rain-flow cycle counting. The PDF labeled "Experiment Dirlik" was calculated from the moments of the experimental 100-s PSD and provided a baseline for comparing the linear and nonlinear FEA-based Dirlik PDFs or "ABAQUS Dirlik" and "ODU Dirlik," respectively. It should be noted that the Dirlik approach is only applicable for linear Gaussian processes. Using the technique for nonlinear systems was done for comparison purposes only. The PDFs displayed in Fig. 9 were then used with Miner's damage accumulation model [Eqs. (12) and (18)] and the material constants $K = 3.89\text{E}24$ and $\alpha = 0.212$ from a log-log S-N curve to estimate the fatigue life. K and α were derived from random vibration 9-bay stiffened panel tests, with stress monitored in the center panel along the midpoint of the long span rivet line.[15] The resulting estimates are displayed both in Fig. 9 and Table 2. Examining Fig. 9, there are several conclusions that can be made. First, there is good correlation between the experimental results and the experimental-based fatigue life predictions, although it should be noted that only two panels were fatigue tested. The "Experimental Dirlik" PDF provided the most accurate approximation to the rain-flow results. However, the technique overpredicted the panel life by 11%. Note the disparity between the FEA PDFs and experimental-based rain-flow PDF life estimates. The FEA-based Dirlik PDFs and resulting fatigue life estimates of 75.27 and 343.2 s were too conservative compared with the experimental fatigue estimates of 1394-, 1260-, and the 1270-s estimate from the rms fundamental frequency failure criterion, although the nonlinear FEA results were a significant improvement over the linear prediction. This was expected, because of the overly conservative FEA random response results displayed in Fig. 8. Although the ODU analysis incorporates the quadratic and cubic geometric nonlinear stiffness terms, the results indicate that the predicted response is overly compliant (rms value of 737 vs the experimental 563 $\mu\varepsilon$) and also overpredicts the panel geometric nonlinear effects at the fatigue test level. This is noted in Fig. 8, where the response PSD peaks are broader than the experimental results and the natural frequencies of the panel are significantly higher than the experimental results at the same fatigue test level. Possible sources of error include the already mentioned transverse strain gauge sensitivity, as well as the chosen experimental sampling rate. The choice of sampling rate resulted in the use

Table 2 Fatigue life estimates

Method	Estimate, s
5% fundamental frequency drop	1270
Experiment rainflow	1260
Experiment Dirlik	1394
ABAQUS Dirlik	75.27
ODU Dirlik	343.2

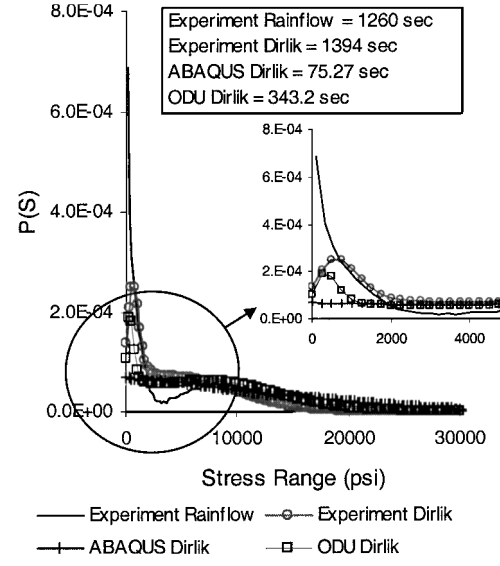

Fig. 9 Dirlik and rain-flow PDFs and resulting fatigue life estimates for 60-g rms input excitation.

of only a single numerical integration time step. Finally, tradeoffs were made between mesh refinement and computational time when considering the nonlinear analysis.

Conclusions

Results show that all of the experimental PDF-based fatigue life estimates compare well to the measured experimental time to failure of 1270 s. Furthermore, both the linear and nonlinear finite element analyses resulted in overly conservative estimates of the fatigue life. Preliminary results indicate that when estimating the fatigue life using a spectral-based PDF technique the principal limit to the analysis is the accuracy of the structural response prediction. Both the linear and nonlinear FEA random response compared well with the baseline loading case, although both analyses significantly overpredicted the panel strain response under fatigue loading. The ODU finite element analysis also overpredicted the panel geometric nonlinear response under fatigue loading, resulting in too great a frequency shift and response peak broadening as compared to the experimental results. However, the nonlinear analysis resulted in a marked improvement in life prediction.

References

[1]Miner, M. A., "Cumulative Damage in Fatigue," *Journal of Applied Mechanics*, Vol. 67, No. 12, 1945, pp. A159–A182.

[2]Bishop, N. W. M., and Sherratt, F., "Fatigue Life Prediction from Power Spectral Density Data. Part 1, Traditional Approaches and Part 2, Recent Developments," *Environmental Engineering*, Vol. 2, No. 2, 1989, pp. 11–16.

[3]Wolfe, H. F., Shroyer, C. A., Brown, D. L., and Simmons, L. W., "An Experimental Investigation of Nonlinear Behavior of Beams and Plates Excited to High Levels of Dynamic Responses," WL/FIBG, WL-TR-96-3057, Wright–Patterson, AFB, OH, Oct. 1995.

[4]Ibrahim, R. A., "Nonlinear Random Vibration: Experimental Results," *Applied Mechanics Review*, Vol. 44, No. 10, 1991, pp. 423–446.

[5]Istenes, R. R., Rizzi, S. A., and Wolfe, H. F., "Experimental Nonlinear Random Vibration Results of Thermally Buckled Composite Panels," *Proceedings of the 36th Structures, Structural Dynamic and Materials Conference*, New Orleans, LA, April 1995, pp. 1559–1568.

[6]Ng, C. F., "Nonlinear and Snap-Through Responses of Curved Panels to Intense Acoustic Excitation," *Journal of Aircraft*, Vol. 26, No. 3, 1989, pp. 281–288.

[7]Ng, C. F., and Clevenson, S. A., "High Intensity Acoustic Tests of a Thermally Stressed Plate," *Journal of Aircraft*, Vol. 28, No. 4, 1991, pp. 275–281.

[8]Dhainaut, J. M., Bin, D., Mei, C., Spottswood, S. M., and Wolfe, H. F., "Non-Linear Response of Composite Panels to Random Excitation and Elevated Temperature," *Proceedings of 7th International Conference on Recent Advances in Structural Dynamics*, Southampton, U.K., 2000, pp. 769–784.

[9]Shi, Y., and Mei, C., "A Finite Element Time Domain Modal Formulation for Large Amplitude Free Vibrations of Beams and Plates," *Journal of Sound and Vibration*, Vol. 193, No. 2, 1996, pp. 453–464.

[10]Schudt, J. A., "The Response of Nonlinear Systems to Random Excitation," M.S Thesis, Dept. of Mechanical Engineering, The Ohio State Univ., Columbus, 1991.

[11]Reinhall, P. G., and Miles, R. N., "Effect of Damping and Stiffness on the Random Vibration of Nonlinear Periodic Plates," *Journal of Sound and Vibration*, Vol. 132, No. 1, 1989, pp. 33–42.

[12]Spottswood, S. M., Wolfe, H. F., and Brown, D. L., "The Effects of Record Length on Determining the Cumulative Damage of a Ceramic Matrix Composite Beam," *Proceedings of the 7th International Conference on Recent Advances in Structural Dynamics*, Southampton, U.K., 2000, pp. 785–799.

[13]Bogner, F. K., Fox, R. L., and Schmit, L. A., "The Generation of Inter-Element Compatible Stiffness and Mass Matrices by the Use of Interpolation Formulas," U.S. Air Force Flight Dynamics Lab., AFFDL-TR-66-80, Wright–Patterson AFB, OH, 1996, pp. 396–443.

[14]Wolfe, H. F., and White, R. G., "The Development and Evaluation of a New Multimodal Acoustic Fatigue Damage Model," *Proceedings of the 6th International Conference on Recent Advances in Structural Dynamics*, Southampton, U.K., 1997, pp. 969–980.

[15]Rudder, F. F., and Plumblee, H. E., "Sonic Fatigue Design Guide for Military Aircraft," U.S. Air Force Flight Dynamics Lab., AFFDL-TR-74-112, AD-B004-600L, Wright–Patterson AFB, OH, May 1975, p. 489.